



# 3D numerical simulation of heterogeneous in situ stress field in low-permeability reservoirs

Jianwei Feng<sup>1,2</sup> · Lin Shang<sup>3</sup> · Xizhe Li<sup>4</sup> · Peng Luo<sup>5</sup>

Received: 3 August 2018  
© The Author(s) 2019

## Abstract

Analysis of the in situ stress orientation and magnitude in the No. 4 Structure of Nanpu Sag was performed on the basis of data obtained from borehole breakout and acoustic emission measurements. On the basis of mechanical experiments, logging interpretation, and seismic data, a 3D geological model and heterogeneous rock mechanics field of the reservoir were constructed. Finite element simulation techniques were then used for the detailed prediction of the 3D stress field. The results indicated that the maximum horizontal stress orientation in the study area was generally NEE–SWW trending, with significant changes in the in situ stress orientation within and between fault blocks. Along surfaces and profiles, stress magnitudes were discrete and the in situ stress belonged to the Ia-type. Observed inter-strata differences were characterized as five different types of in situ stress profile. Faults were the most important factor causing large distributional differences in the stress field of reservoirs within the complex fault blocks. The next important influence on the stress field was the reservoir's rock mechanics parameters, which impacted on the magnitudes of in situ stress magnitudes. This technique provided a theoretical basis for more efficient exploration and development of low-permeability reservoirs within complex fault blocks.

**Keywords** Complex fault blocks · 3D heterogeneity · In situ stress prediction · Reservoir model · Nanpu Sag

## 1 Introduction

In situ stress refers to the internal stress within the Earth's crust and is closely related to gravitational and tectonic stresses (Bell 1996; Kang et al. 2010). Knowledge of the in situ stress field of a reservoir is important in petroleum exploration and field development (Finkbeiner et al. 2001;

Bell 2006; Zoback 2007; Tingay et al. 2010; Li et al. 2014; Ju and Sun 2016; Ju et al. 2017), because it can affect permeable fracture aperture and orientation as well as fault sealing. Understanding in situ stresses also plays an important role in solving engineering problems, such as underground excavation design (Mizuta et al. 1987), wellbore stability evaluation (Zoback et al. 2003; Tingay et al. 2009), and the optimization of ground support systems (Sibson 1994; Binh et al. 2007; Liu et al. 2016).

In recent years, low-permeability reservoirs are the subject of considerable research globally due to their potential for containing oil and gas (Nelson 2009; Zeng et al. 2013; Farrell et al. 2014; Lommatzsch et al. 2015; Wang et al. 2018). Hydraulic fracturing is a current trend and an effective method to develop low-permeability reservoirs. During hydraulic fracturing, the form of fractures, method of fracture extension, and production efficiency are greatly influenced by the state of the in situ stress field. The four most important research aspects during the development of low-permeability reservoirs are: (1) changes under stress within the reservoir; (2) deformation and fracturing mechanisms of the rock; (3) optimization of horizontal well trajectories; and (4) hydraulic fracturing design (He et al. 2015; Hoda

Edited by Jie Hao and Xiu-Qiu Peng

✉ Jianwei Feng  
Linq\_fengjw@126.com

✉ Xizhe Li  
lxz69@petrochina.com.cn

<sup>1</sup> School of Geosciences, China University of Petroleum (Huadong), Qingdao 266580, Shandong, China

<sup>2</sup> Shandong Provincial Key Laboratory of Reservoir Geology, Qingdao 266580, Shandong, China

<sup>3</sup> Exploration and Development Research Institute, PetroChina Jidong Oilfield Company, Tangshan 063004, Hebei, China

<sup>4</sup> Research Institute of Petroleum Exploration and Development, Beijing 100083, China

<sup>5</sup> Saskatchewan Research Council, Regina, SK, Canada

et al. 2015). In situ stress is one of the most significant characteristics when assessing these key factors. Comprehensive research of in situ stress in reservoirs by using various methods is important (Zeng et al. 2013; Zoback et al. 2003).

The most direct and effective means of determining in situ stress is well site measurements and the acquisition of core for testing. Core testing includes paleomagnetic orientation, wave velocity anisotropy, acoustic emission, and differential strain; field measurement methods include borehole breakouts, drilling-induced fractures, and downhole microseismic monitoring. These methods can be used to obtain the magnitude and orientation of in situ stress (Dai 2002; Zoback 2007; Zang and Stephansson 2009; Zhang et al. 2012; Eshiet and Sheng 2018). These techniques are relatively well developed and widely applied. Various models to calculate the in situ stress of heterogeneous strata have been proposed using well logging data (Wang et al. 2008; Chen et al. 2009a; Fan et al. 2009), to obtain one-dimensional and continuous in situ stress data for entire well sections. In recent years, with rapid development of digital technology, a digital volumetric speckle photography (DVSP) technique has been developed to quantitatively record and measure the three-dimensional (3D) deformation and strain field inside rocks under load (Chen et al. 2005; Chiang and Mao 2015). Further, Mao et al. (2015a, b) and Lu (2016) apply the DVSP technique in combination with X-ray micro-tomography to obtain the 3D interior strain fields in a sandstone specimen under uniaxial compression, and has achieved good research results. However, this technique is still difficult to measure the 3D strain field under confining pressure, so it can only supplement or verify the numerical simulation of stress.

There is still a lack of a mature analytical methods and techniques for predicting the distribution of inter-well in situ stress, especially in regions with complex fault blocks and highly heterogeneous stress fields. At present, the main methods for predicting in situ stress fields are two-dimensional (2D) or 3D numerical simulations using the finite element method (FEM) and wells as constraints (Xie et al. 2008; Liu et al. 2009; Tian et al. 2011; Yang et al. 2012; Yu et al. 2016; Mao et al. 2015a, b; Dai et al. 2016). The former is mainly used for large-scale basin modeling. It focuses on predicting in situ stress orientation and is qualitative to semiquantitative studies of in situ stress magnitudes. The latter can reflect the distribution of the stress field within target strata in 3D space. However, prediction accuracies are largely dependent on the construction of the geological model and determination of the rock mechanics parameters.

Previous studies used digital processing of the tectonic map of the target layers to obtain the layers 3D coordinates (Wang et al. 2007, 2016; Dai et al. 2011, 2014; Ding et al. 2011, 2016; Lei et al. 2015). However, the precision of digitization is low, resulting in oversimplification of faults. Furthermore, the mechanical models used are stratified

horizontally and have homogeneous planes, meaning that well-constrained rock mechanics parameters are used as substitutes for the rock mechanics parameters of a particular area, or even an entire region (Zhu et al. 2016). Such approaches do not meet the requirements for understanding the in situ stress field of reservoirs within complex fault blocks.

This study examined a deep-buried reservoir in the No. 4 Structure of Nanpu Sag. The reservoir lithology is dominated by low-permeability sandstones located within complex fault blocks. This significant region within the larger Jidong Oil field is currently the focus of exploration and development. The reservoir is characterized by highly variable lithofacies, variable fluid properties, low porosity, low permeability, and high heterogeneity and anisotropy (unpublished data from the PetroChina Jidong Oil field Company 2017). The reservoir is cross-cut by a large number of faults. Exploration and development of the region have been mostly slow and inefficient due to the poor geological conditions and inadequate exploitation techniques. Hence, research on the in situ stress of No. 4 Structure of Nanpu Sag can provide technical support for well planning and the design of fracturing schemes (Cao 2005; Haghi et al. 2013). This can help to improve the outcomes of reservoir exploration and development.

In view of the aforementioned issues, this study enhances and innovates the approach in two ways: (1) using the technique of seamlessly welding the geological and FEM models, that is, using a combined Petrel and ANSYS modeling technique, to more accurately model the actual undulations of the target strata in the study area and to make detailed depictions of the 3D form of faults; and (2) using a combination of core tests and geophysical methods to construct a 3D heterogeneous rock mechanics model of the target strata. These can be used to predict the distribution of in situ stress in the No. 4 Structure of Nanpu Oil field and to provide suggestions for optimum well pattern design within the strata for fracturing.

## 2 Background and overview

### 2.1 Overview of study area

The Bohai Bay Basin, an important hydrocarbon-producing province in China, is located on the eastern coast of China and covers an area of approximately 200,000 km<sup>2</sup>. It appears as a northeast-trending ‘‘lazy-Z’’ pattern (Mann et al. 1983) on the regional geologic map (Dong et al. 2010) (Fig. 1a). It consists of six major depressions, including Liaohe, Bozhong, Jiyang, Jizhong, Huanghua, and Linqing depressions (Gong 1997) (Fig. 1b). The northeast part of the Huanghua depression contains the Nanpu Sag, the northern

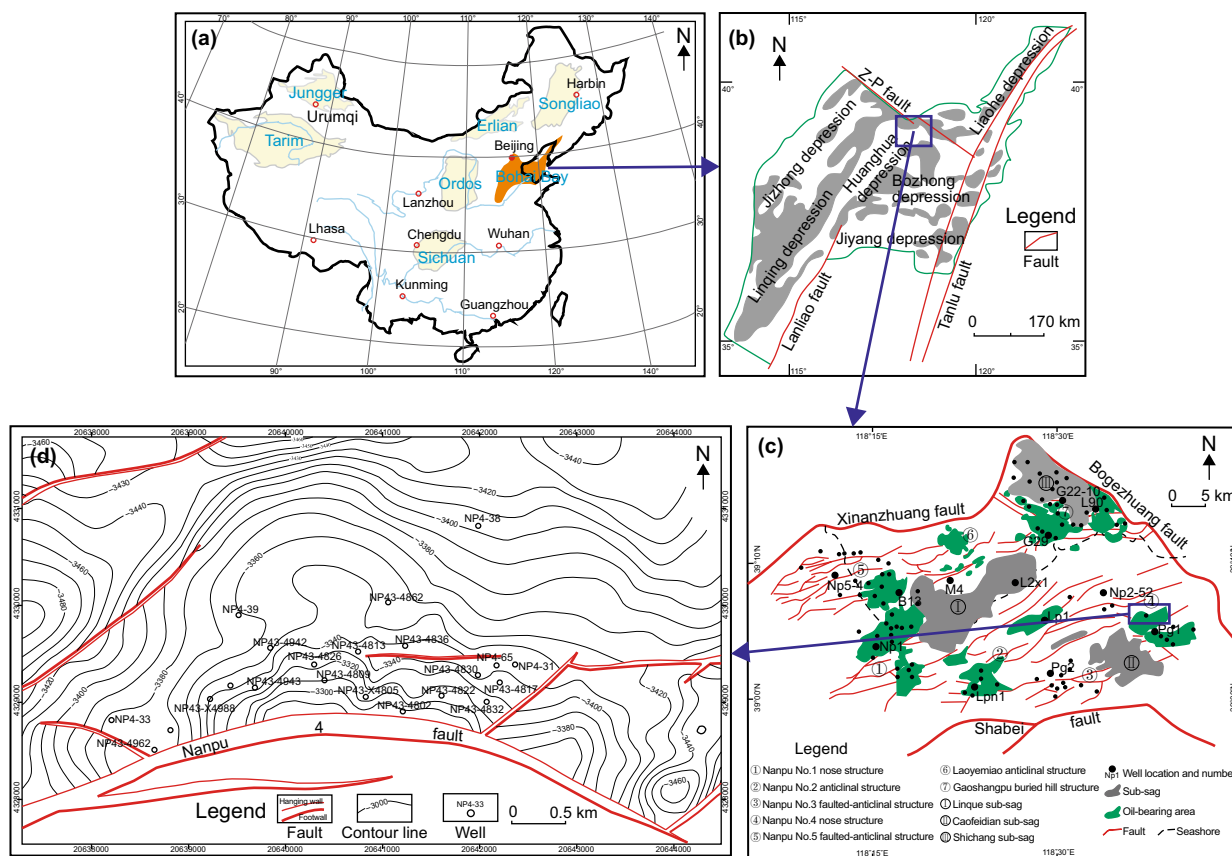


**Fig. 1** **a** Map showing the outline of the Bohai Basin. **b** Map of the Bohai Basin showing the major faults and location of the study area. **c** Map of the Nanpu Sag showing faults and hydrocarbon distribution. **d** Map of the study area showing the fault block structure of the No. 4 area/Structure. Contours represent the top surface of  $Ed_{2+3}$

region of which in turn contains the 1930 km<sup>2</sup> Nanpu Oil field. This oil field’s deep reservoir is sited within a region of complex fault blocks, formed by the Gaolin Fault and its derivative faults (Zhang 2010). The main oil–gas reservoir is located in the  $Ed_{2+3}$  members, which mainly consist of fine sandstone, argillaceous sandstone and mudstone. The Nanpu Oil field is divided into five structural blocks by the Gatuo fault and Gaoliu fault (Fig. 1c). In the No. 4 Structure, NE–SW and NW–SE striking faults developed in a reticulate pattern, dividing the area into multiple fault blocks that are nearly rectangular or rhombic in shape. The No. 4 Structure is dominated by NE–SW/NW–SE striking curved fault (i.e., Nanpu.4 fault) that derives several secondary radial faults oriented in multiple directions (Fig. 1d). About 70% of the reservoir is oil-bearing area and under exploitation. In the second section of the Dongying Formation in this reservoir is the  $Ed_2$  member, which is currently the focus for exploration and development in the Jidong Oil field.

The No. 4 Structure’s  $Ed_{2+3}$  members contain five oil series, which are labeled as I, II, III, IV, and V from top to bottom. The layers are buried at a depth of 3200–3400 m and comprise mainly distributary channel sand bodies of

subaqueous fan deltas. Its average porosity and permeability are 14.3% and 3.8 mD, respectively, giving the reservoir the characteristics of medium/low porosity and low/ ultra-low permeability. In addition, the No. 4 Structure has poor physical properties and high heterogeneity, and the tectonic fracture development level is low. After many years of waterflooding operations, the oil field is currently being reassessed for the development of a well pattern.

### 2.2 In situ stress tensor

In general, the state of in situ stress can be described by the stress tensor, which includes the orientation and magnitude of the three orthogonal principal stresses (Engelder 1993). In general, three types of in situ stress regime are determined based on the relative magnitude of the minimum horizontal stress ( $S_{hmin}$ ), maximum horizontal stress ( $S_{Hmax}$ ) and vertical stress ( $S_V$ ) (Anderson 1951): (i) Normal faulting stress regime:  $S_V > S_{Hmax} > S_{hmin}$ ; that is, I-type; if  $S_{hmin} > 0$ , it belongs to the Ia-type; if  $S_{hmin} < 0$ , it belongs to the Ib-type.

- (ii) Strike-slip faulting stress regime:  $S_{Hmax} > S_V > S_{hmin}$ .
- (iii) Reverse faulting stress regime:  $S_{Hmax} > S_{hmin} > S_V$ .

Stress coefficients are important parameters used for describing in situ stress. These include the ratio of the  $S_{H_{\max}}$  to  $S_{H_{\min}}$  ( $k_{H/h}$ ), lateral pressure coefficient ( $k$ ), and  $S_{H_{\max}}$  and  $S_{H_{\min}}$  horizontal stress coefficients ( $k_H$  and  $k_h$ , respectively) (Brown and Hoek 1978; Savage et al. 1992; Engelder 1993; Tingay et al. 2010). Equation 1 can be used to calculate the relationship between the various stress coefficients:

$$\begin{cases} k_{H/h} = S_{H_{\max}}/S_{H_{\min}} \\ k = (S_{H_{\max}} + S_{H_{\min}})/(2S_V) \\ k_H = S_{H_{\max}}/S_V \\ k_h = S_{H_{\min}}/S_V \end{cases} \quad (1)$$

The stability of the reservoir rock is affected by  $K_{H/h}$ , which is similar to the horizontal differential stress ( $S_{H_{\max}} - S_{H_{\min}}$ ). The larger the ratio, the more unstable the rock tends to be (Li et al. 2011b). This causes fractures to extend along the orientation of  $S_{H_{\max}}$ , such that it would be difficult for complex reticulated fractures to form. The coefficient  $k$  is used to describe the horizontal stress being borne by the underground rock mass and is the direct manifestation of the horizontal load at the borehole wall. Both  $K_H$  and  $K_h$  describe the relationship between the horizontal and vertical stresses. The stress coefficients and depth cross-plots can show the general trend of horizontal in situ stress to increase with depth. This provides supplementary information on the spatial distribution of in situ stress, and provides reference values for the estimation of in situ stress for regions that lack in situ stress data.

Affected by the Pacific plate, Philippine plate, Indian Ocean plate and Siberian plate, the direction of the modern tectonic stress field in China can be divided into three regions: The west is mainly squeezed by the nearly south–north (S–N) direction, and the direction of  $S_{H_{\max}}$  is nearly S–N (Liu et al. 2006; Dai et al. 2013). The stress state in the west belongs to a compression type or type II geostress state. The eastern part (e.g., the Bohai Bay Basin) is mainly subject to near SW–NE compression, the direction  $S_{H_{\max}}$  is nearly SW–NE, and the corresponding stress state belongs to a type Ia geostress state (Ju et al. 2016). As a transitional zone, the stress state in the middle part is mainly a strike-slip type, or type III geostress state. As the plate boundary of eastern China, the Tanlu fault is a deep fault zone dominated by shearing movement, and it has recently inherited some of the characteristics of neotectonic movement (Zeng et al. 2001; Shui et al. 2016). For Cenozoic activities of the Tanlu fault zone, most researchers believe that right-lateral strike-slip extension and left-lateral strike-slip extrusion have occurred since Paleogene, and nowadays they are still dominated by right-lateral strike-slip extrusion (Zeng et al. 2001; Shui et al. 2016; Yang et al. 2017). Therefore, in

general, the current stress field of Nanpu Sag is dominated by nearly SW–NE compression, and is also affected by the eastern fault, showing a coexisting right-lateral strike-slip characteristic.

### 3 Methodology and input data

#### 3.1 Characteristics of in situ stress at the key wells

##### 3.1.1 Orientation of in situ stress by borehole breakouts

Practical experiences have shown that the directional orientation of the in situ stress can be determined according to the orientation of the borehole breakouts (Bell and Gough 1979; Dai 2002; Zoback et al. 2003). Rock removed from the subsurface when a well is drilled no longer supports the surrounding rock, resulting in concentrated stresses (Plumb and Hickman 1985; Rajabi et al. 2010). Borehole breakouts happen when the stress exceeds that required to cause rock failure, with the orientation of the borehole breakouts representing the orientation of the minimum horizontal stress ( $S_{H_{\min}}$ ) (Bell and Gough 1979; Zoback et al. 2003; Brooke-Barnett et al. 2015; Fig. 2a). Generally, borehole breakouts in image logs appear as broad, parallel and often poorly resolved conductive zones separated by 180° with caliper enlargement in the direction of the conductive zones (Bell 1996; Rajabi et al. 2010; Tingay et al. 2010; Kingdon et al. 2016). For example, the Fullbore Formation Microimager (FMI) logs of an interval of borehole breakout in well NP4-31 (Fig. 2a), showed the orientation of the breakouts to be N–S, indicating that the maximum horizontal stress ( $S_{H_{\max}}$ ) was in an E–W orientation. After determining the orientations of borehole breakouts for nine wells, we determined the  $S_{H_{\max}}$  of the No. 4 Structure to be between NEE–SWW and SEE–NWW (Fig. 2b). The image logs and data were obtained from Jidong Oil Company reports.

##### 3.1.2 In situ stress magnitude by acoustic emission (AE)

The acoustic emission method is generally used to determine paleo-tectonic stresses experienced in rocks, and can also be used to acquire the magnitude of in situ stress (Holcomb 1993; Chen et al. 2009b; Li et al. 2011a; Lehtonen et al. 2012; Zhao et al. 2012). Brittle materials retain memory of the loading effect that they have been subjected to (Zang and Stephansson 2009). The stress history of the rock could be analyzed on the basis of this ability. According to the definition of Kaiser effect, the preexisting maximum stress of sampling point is measured by AE method instead of the current stress. However, after a lot of practice, Ding and Zhang (1991) proposed the concept of “visual Kaiser effect.” In detail, AE method/curve can obtain two Kaiser points,

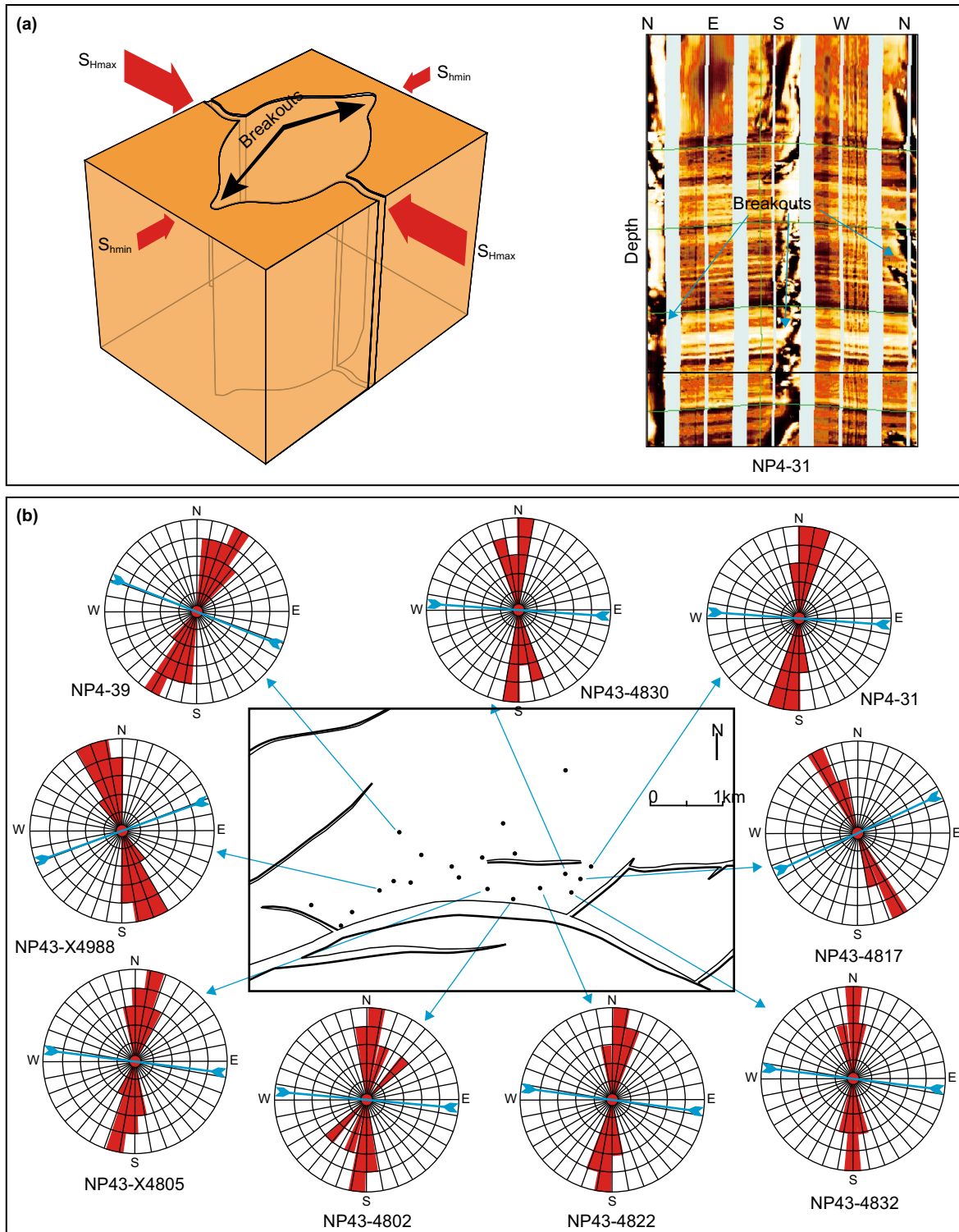


**Fig. 2** **a** Borehole breakout as observed in (left) schematic borehole and (right) image logs (an example from well NP4-31). **b** The azimuth histograms show the orientation of borehole breakouts and the blue arrows indicate the  $S_{Hmax}$  orientation, namely the compression direction

one corresponding to the stress causing the saturated saturation of the rock. It is consistent with the current stress field and lower than the historical maximum stress value, so it is

called the visual Kaiser point. On AE curve, after the visual Kaiser point, another true Kaiser point is obtained, which corresponds to the highest historical stress. From above, the

load stress experienced by rock samples in different directions (*X* direction, *Y* direction, *XY* direction and *Z* direction) could be evaluated (Fig. 3a), and the values of in situ stress are analyzed using the following equations.

$$\begin{cases} \sigma_v = \sigma_{\perp} \\ \sigma_H = \frac{\sigma_x + \sigma_y}{2} + \sqrt{\left(\frac{\sigma_x - \sigma_y}{2}\right)^2 + (\sigma_{x45y} - \frac{\sigma_x + \sigma_y}{2})^2} \\ \sigma_h = \frac{\sigma_x + \sigma_y}{2} - \sqrt{\left(\frac{\sigma_x - \sigma_y}{2}\right)^2 + (\sigma_{x45y} - \frac{\sigma_x + \sigma_y}{2})^2} \end{cases} \quad (2)$$

where  $\sigma_{\perp}$  is the in situ stress component of the *Z* direction,  $\sigma_x$  is the in situ stress component of the *X* direction,  $\sigma_{x45y}$  is the in situ stress component of *XY* direction and  $\sigma_y$  is the in situ stress component of *Y* direction.

In this study, 9 groups of AE test were conducted at Shandong University of Science and Technology (Fig. 3b). The test results are shown in Table 1. In situ stress magnitude in the No. 4 Structure varied widely. The respective values for  $S_{Hmax}$  and  $S_{hmin}$  were 66.0–79.5 MPa and 53.9–75.5 MPa; those for vertical principal stress and horizontal differential stress were 72.5–84.4 MPa and 5.52–13.14 MPa. The overall distribution of in situ stress exhibited the trend of being lower in the west and higher in the east.

### 3.2 Detailed prediction of a 3D heterogeneous stress field

An outline of the workflow behind the detailed prediction of a 3D heterogeneous stress field is shown in Fig. 4. First, the 3D visualization modeling software Petrel was used to build a 3D geological model of the target layer in the study area from drilling, logging, seismic, and regional geological

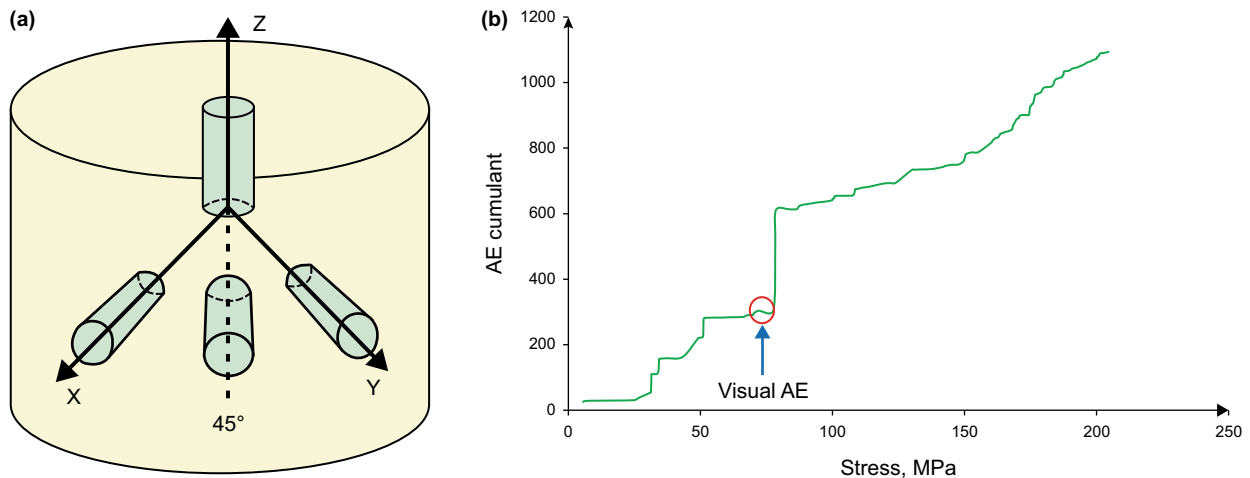


**Fig. 3** **a** Sampling for acoustic emission from various directions (*X* direction, *Y* direction, *XY* direction, and *Z* direction). **b** Cumulative acoustic emission graph used to determine the magnitude of in situ stress (an example of sample from *Y* direction in well NP43-4862, where stress magnitude at the point labeled visual AE is 81.02 MPa)

**Table 1** Error analysis of simulation results of the in situ stress

Well number	$\sigma_H$ , MPa			$\sigma_h$ , MPa			$\sigma_v$ , MPa			$\sigma_H - \sigma_h$ , MPa		
	M	S	E	M	S	E	M	S	E	M	S	E
NP4-65	66.0	67.4	1.4	59.5	53.3	6.2	72.5	78.2	5.7	6.5	14.1	7.6
NP4-31	70.1	65.7	4.4	59.8	52.2	7.6	72.1	78.6	6.5	10.3	13.5	3.2
NP43-X4805	79.5	77.5	2	63.3	64.5	1.2	84	83.4	0.6	16.2	13	3.2
NP43-X4830	78.5	76.4	2.1	60.3	51.8	8.5	84.4	89.1	4.7	18.2	24.6	6.4
NP43-4832	63.5	65.4	1.9	53.9	50.0	3.9	82.0	84.3	2.3	9.6	15.4	5.8
NP43-4862	69.4	66.3	3.1	64.7	60.1	4.6	74.5	78.2	3.7	4.7	6.2	1.5
NP4-33	81.2	79.3	1.9	67.2	62.9	4.3	82.6	85.7	3.1	14	16.4	2.4

*M* measured, *S* simulation, *E* error

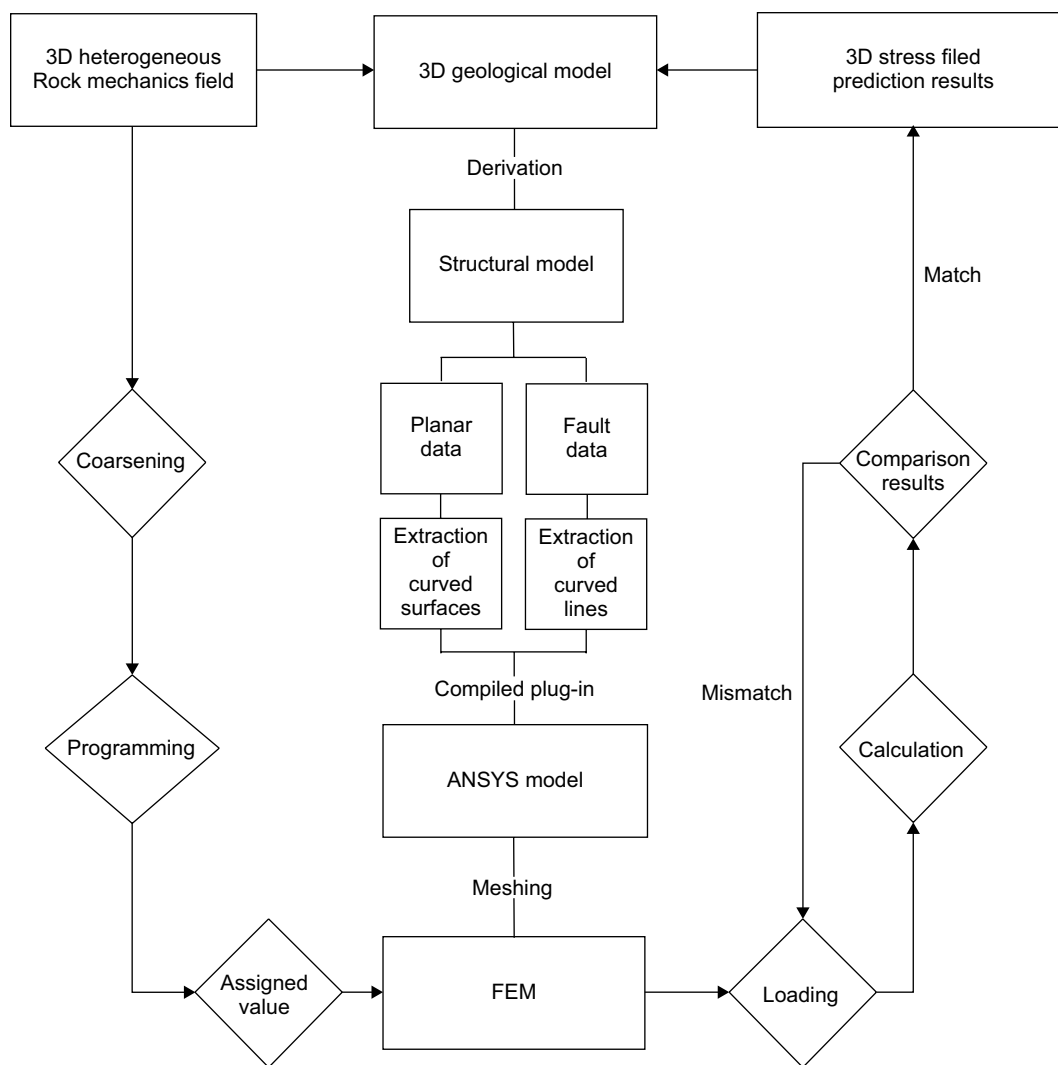


Fig. 4 Flowchart for detailed prediction of 3D heterogeneous stress field

data. After surface and fault data were derived for the target stratum, AutoCAD software was used to extract the curved surfaces and lines and for model reconstruction. A standalone application that we developed converted the model into a format (iges) recognized by ANSYS software, which enabled the model to be imported into ANSYS.

The results of rock mechanics experiments were used as constraints and combined with geophysical methods to construct a 3D rock mechanics field model. The 3D heterogeneous rock mechanics parameters were then assigned to each grid of the FEM model by programming. The test results of in situ stress in key wells were used as constraints and combined with the geotectonic background of the study area to determine the appropriate constraints and loaded for application to the model. The results were automatically calculated by ANSYS software. By seamlessly welding the geological and FEM models, the stress field prediction results obtained

from numerical simulation were treated as a type of geological information, and re-imported into the 3D geological model. This allowed the prediction results for stress field to be analyzed.

### 3.2.1 Geological modeling and rock mechanics field

The geological model consisted of the structural model, its attributes, and related geological information; the structural model included the surface and fault models. The No. 4 Structure’s current 3D structural model consisted of 8 faults and the surfaces of five oil series. The area was a monoclinic structure that dips in north and was divided into multiple fault blocks. The faults were of various sizes, with fault spacings of about 20–100 m, and dip magnitudes were mainly greater than 60°. All faults in the study area belonged to the normal fault type (Figs. 1c and 6a).

The rock mechanics parameters include Young’s elastic model, Poisson’s ratio, and rock density, all of which are prerequisite for in situ stress research. Logging data were used to explain the continuous rock mechanics parameters of a single well’s profile. The calculation method is as follows (Wang et al. 2014; Lu et al. 2015):

$$E_d = \frac{\rho_b}{\Delta t_s^2} \cdot \frac{3\Delta t_s^2 - 4\Delta t_p^2}{\Delta t_s^2 - \Delta t_p^2} \tag{3}$$

$$\mu_d = \frac{\Delta t_s^2 - 2\Delta t_p^2}{2(\Delta t_s^2 - \Delta t_p^2)} \tag{4}$$

where  $E$  is the Young’s elastic modulus, MPa;  $\mu$  is the Poisson’s ratio, dimensionless;  $\rho_b$  is the rock density, kg/m<sup>3</sup>; and  $\Delta t_p$  and  $\Delta t_s$  are the time differences of the longitudinal and transverse waves, respectively,  $\mu$ s/ft.

The parameters for elasticity calculated from logging data are dynamic parameters, which vary to a certain extent from the static parameters for elasticity. Since the latter are more suitable for petroleum engineering projects, a conversion relationship was established as a dynamic–static parameter correction (Fig. 5a, b). Static parameters were obtained from the results of rock mechanics experiments. Correction for rock density was not required because it is less affected by experimental and calculation methods.

The 3D distributions of the No. 4 Structure’s rock mechanics parameters were obtained after the seismic interpretation and integration of the area’s seismic attributes (Fig. 6a). The elastic modulus varied mainly between 24–42 GPa (Fig. 6b), and Poisson’s ratio was concentrated between 0.2–0.27 (Fig. 6c). In the 3D space, the rock density was between 2.05 and 2.60 g/cm<sup>3</sup> (Fig. 6d). Differences in the rock mechanics parameters within and between fault blocks were clear. The mechanical

parameters of the fault zone have a great influence on the results of stress modeling, but the current accurate acquisition of parameters is still a problem. Generally, the size of the grid in modeling software is larger than 20 m, but the width of most faults in study area is smaller than this value. Therefore, it is difficult to accurately reflect the change of mechanical parameters of fault zones by seismic attribute technique. According to previous studies, the fault zone can be defined as a weak/soft zone, and its mechanical parameters are different from those of the surrounding rocks (e.g., Liu et al. 2008; Jiu et al. 2013). Commonly, the Young’s modulus of fault zones is 50%–70% of the surrounding rocks or normal sedimentary stratum. Moreover, the Poisson’s ratios in fault zones were larger than those of the corresponding sedimentary rock stratum, and their differences were typically between 0.02 and 0.10 (Guo et al. 2016). From above, the 3D mechanical parameters obtained from the seismic attributes were finally adjusted and corrected to obtain heterogeneous mechanical parameters of fault zones. In order to ensure the effective assignment of parameters, the volumetric centroid method was used to transform the 3D mechanical parameters in geological modeling software into finite element simulation platform (ANSYS software).

Since samples from the No. 4 Structure presented brittle deformation characteristics, numerical simulations and calculations were made according to elastomer data. Solid185 is a high-order, 3D, and 20-node solid structural unit in ANSYS that can better simulate irregular grid models and comply with the mechanical characteristics of reservoir rocks (Wang 2014). Hence, it was used as the unit type for faults and strata. After simulation accuracy and computational efficiency of the model were taken into consideration, the step size of the fault grid and the strata with its surrounding rocks were set to 300 and 500, respectively. The model was divided into 224,528 nodes and 1,323,943 mechanical units (Fig. 7a).

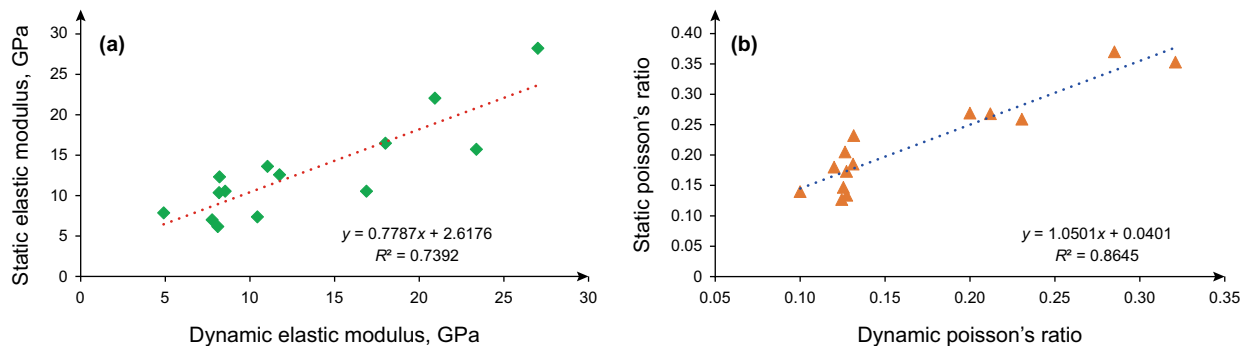


**Fig. 5** Linear regression models used as the dynamic–static correction parameters for the elastic modulus and Poisson’s ratio. **a** Correction model between dynamic elastic modulus and static elastic modulus. **b** Correction model between dynamic Poisson’s ratio and static Poisson’s ratio



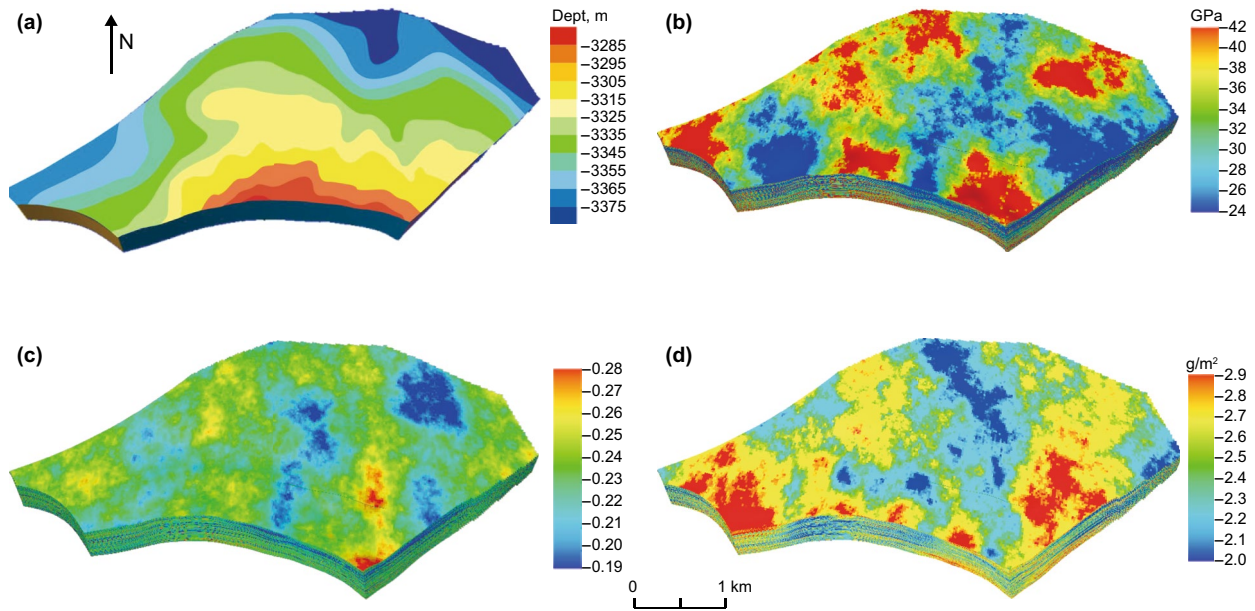


**Fig. 6** Structural models of the No. 4 Structure and its 3D rock mechanics parameters. **a** The 3D geological model of the No. 4 Structure. **b** The elastic modulus model. **c** The Poisson's ratio model. **d** The rock density model

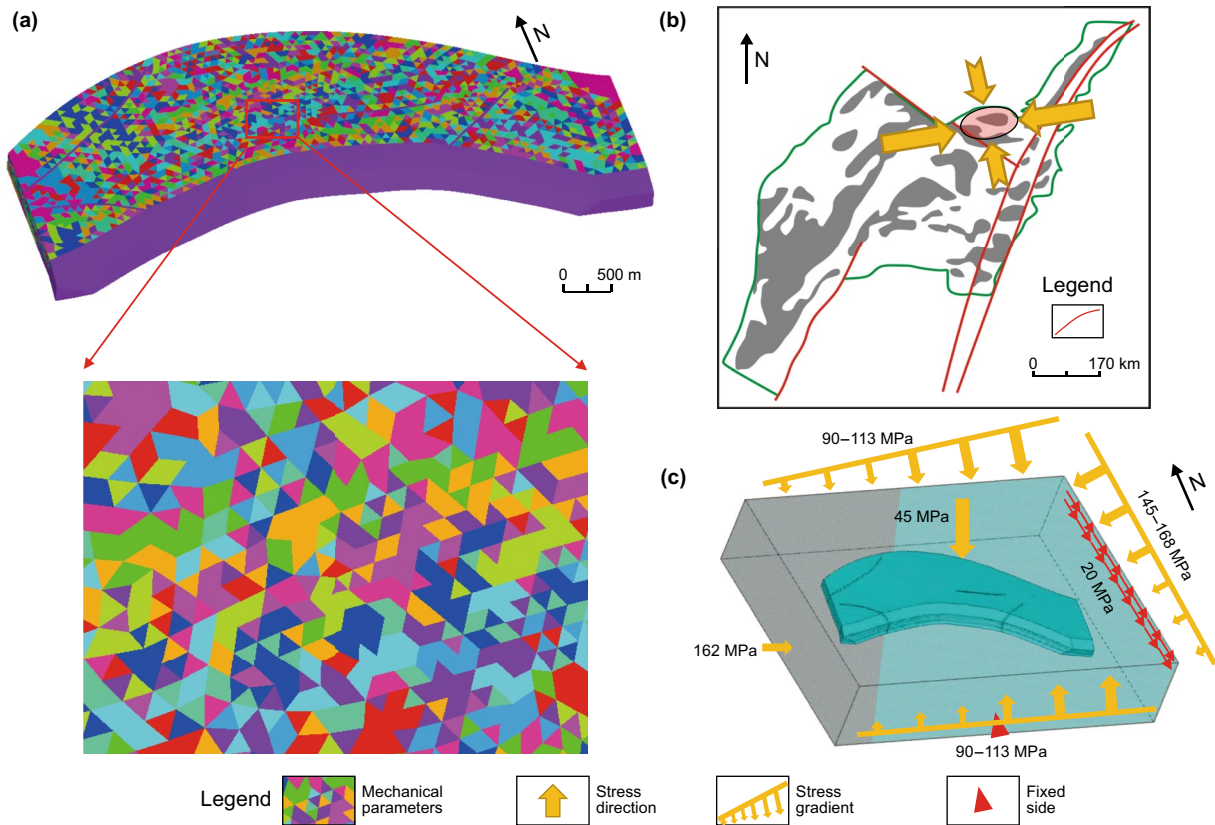


**Fig. 7** **a** Mechanical elements of 3D stress field; in adjacent elements, the colors represent different mechanical attributes. **b** Geotectonic background. **c** Setting of boundary conditions

### 3.2.2 Boundary conditions

Boundary conditions affect the accuracy of numerical simulations of the stress field. On the basis of the results discussed in Sect. 3.1.1, a simplified NEE orientation was taken as the orientation of the principal compressive stress in the study area. As such, the side of external frame surrounding the target area model was aligned to be parallel to that orientation. Next, with the regional tectonic background as the constraint, the boundary of target area model was also determined (Fig. 7b).

After multiple trial calculations, boundary conditions of the model were ascertained. A pressure of 85 MPa was applied to the western boundary, and pressure gradients of 90–113, 90–113, 90–113, and 145–168 MPa were exerted onto the western, northern, southern, and eastern boundaries, respectively (Fig. 7c). Concurrently, a right-lateral strike-slip of 20 MPa was applied to simulate the impact of the Tanlu fault zone. Another 45 MPa of pressure was exerted in the downward vertical direction based on rock mass gravity.

### 3.2.3 Simulation results

The distributional characteristics of the in situ stress in the No. 4 Structure were obtained using FEM simulations and calculations. These included the orientations and magnitudes of  $S_{Hmax}$  and  $S_{Hmin}$  ( $\sigma_H$  and  $\sigma_h$ , respectively), vertical principal stress ( $\sigma_V$ ), and horizontal differential stress ( $\sigma_H - \sigma_h$ ). The simulation and measured results were then compared (Figs. 8 and 9, Table 1). The average errors for the magnitudes of the  $S_{Hmax}$  and  $S_{Hmin}$  were 2.4 and 5.18 MPa, respectively; the average errors for the values of the vertical

principal stress and horizontal differential stress were 3.8 and 4.3 MPa, respectively.

## 4 Results and discussion

### 4.1 The distribution of in situ stress orientations

The overall orientation of  $S_{Hmax}$  in the No. 4 Structure was NEE–SWW to SEE–NWW with a measured range between  $58^\circ$ – $238^\circ$  and  $103^\circ$ – $283^\circ$ . In the central region of the study area, the orientation of  $S_{Hmax}$  was closer to E–W, between  $75^\circ$ – $255^\circ$  and  $96^\circ$ – $276^\circ$ . In the western region, the orientation of  $S_{Hmax}$  was closer to NE–SW, between  $58^\circ$ – $238^\circ$  and  $88^\circ$ – $268^\circ$ . In contrast, orientations in the eastern region gradually rotated toward the SE–NW ( $99^\circ$ – $279^\circ$ ; Fig. 8). The orientations of  $S_{Hmin}$  and  $S_{Hmax}$  were perpendicular, and the overall  $S_{Hmin}$  orientations were from NNW–SSE to NNE–SSW.

Within a fault block, the orientation of  $S_{Hmax}$  was relatively uniform and the variations were even. In contrast, changes in orientation were most obvious between different fault blocks. The non-uniform stress orientations were caused mainly by lithofacies heterogeneity and fault distribution. The former caused small, but consistent changes in the stress orientation within a fault block; the latter caused obvious deflections of the stress orientation. Consequently, there were large differences in stress orientation between fault blocks on either side of a fault.

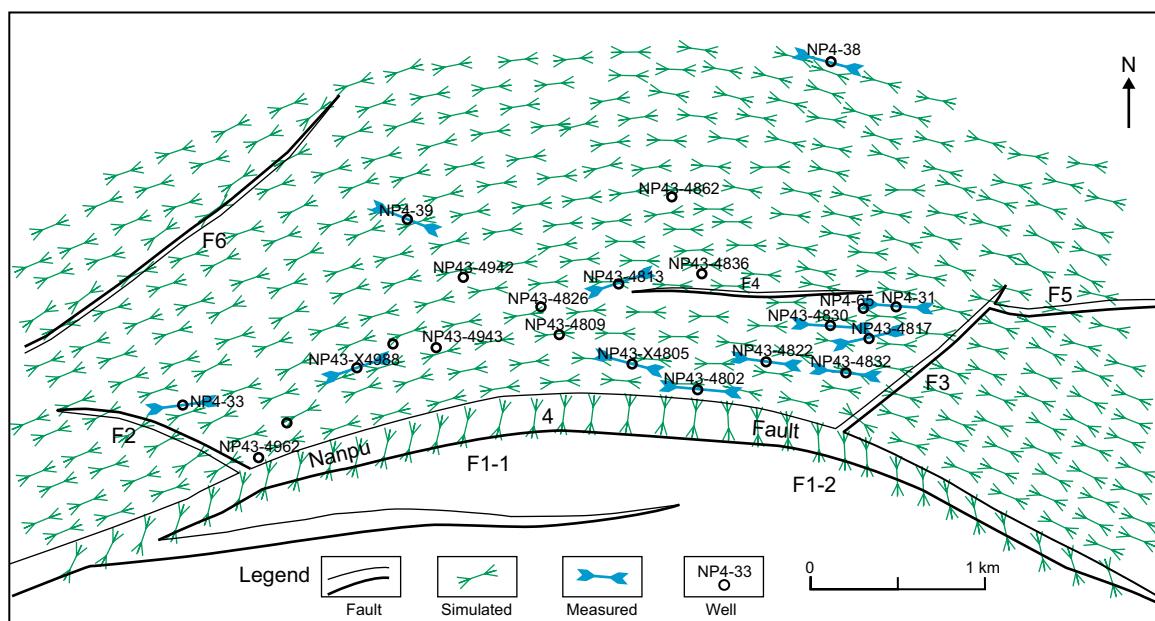
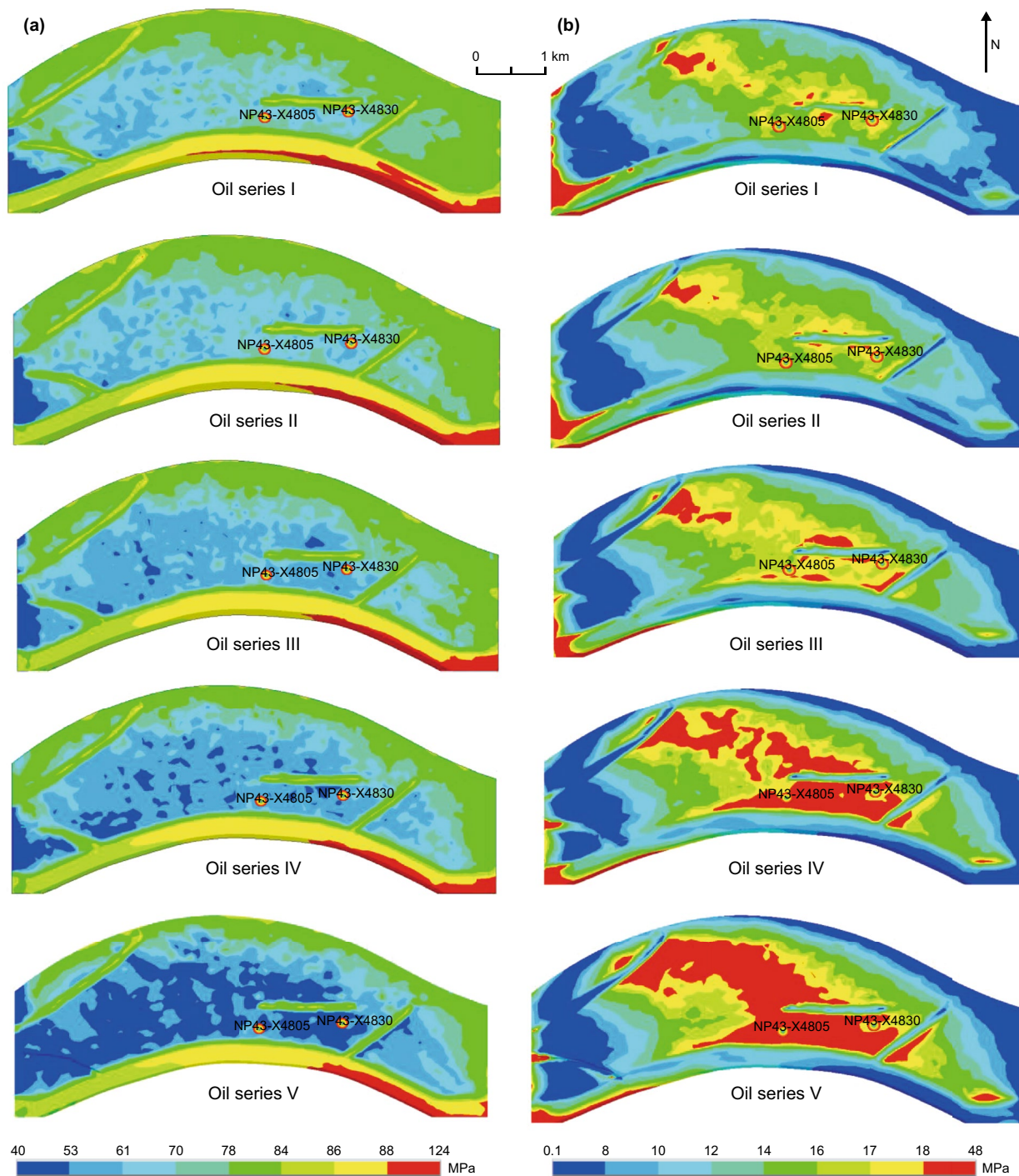


Fig. 8 Measured and simulation results for the orientation of  $S_{Hmax}$  in the No. 4 Structure



**Fig. 9** Simulation results of the stress field in the No. 4 Structure for each of the oil series strata. **a** Simulation results of  $S_{Hmax}$ . **b** Simulation results of horizontal differential stress

The degree of deflection in stress orientation was related to the attribute parameters of the fault, which included its scale (mainly the fault’s slip), strike, filling material, and morphology. The angle between fault strike and regional principal stress was the main factor that caused deflections in the in situ stress field in the No. 4 Structure. When fault

strike and regional  $S_{Hmax}$  formed angles of  $30^{\circ}$ – $60^{\circ}$ , the deflection angle of  $S_{Hmax}$  was the largest. The deflection was also oriented toward the fault orientation. Nanpu.4 Fault (fault F1) is curved boundary fault of the No. 4 Structure with strike gradually varying from approximately NE–SW to NW–SE ( $68^{\circ}$ – $248^{\circ}$  to  $129^{\circ}$ – $309^{\circ}$ ; Fig. 8). Further, according

to the trend change, this main fault could be divided into the two sections: the western section (F1-1) and the eastern section (F1-2). Since the regional  $S_{H_{max}}$  was oriented NEE–SWW ( $80^{\circ}$ – $260^{\circ}$ ), the angles between it and the sections of fault were about  $12^{\circ}$  and  $49^{\circ}$ , respectively. Hence, the orientation of  $S_{H_{max}}$  was drastically deflected along the eastern section (F1-1) in the northern large area of Nanpu-4 fault. Similarly, under the influence of fault F3 and fault F6 (with angles of  $37^{\circ}$  and  $32^{\circ}$ , respectively), the stress directions near the faults also changed to some extent.

When the regional  $S_{H_{max}}$  and a fault's strike were either nearly parallel or perpendicular, meaning that the angle between them was either smaller than  $30^{\circ}$  or greater than  $60^{\circ}$ ,  $S_{H_{max}}$  showed a very small deflection or no deflection at all. The strike of the western section fault F1 was NE–SW ( $68^{\circ}$ – $248^{\circ}$ ) and formed an angle of about  $12^{\circ}$  to  $S_{H_{max}}$ , and the strike of faults F4 and F5 were nearly perpendicular (Fig. 8). Thus, near these three faults, there was no obvious deflection in the orientation of  $S_{H_{max}}$ .

The impact of fault scales on in situ stress was manifested in terms of the magnitude of the fault's slip. The larger the slip, the more obvious was the deflection in in situ stress orientation, and wider the range of the impact. The smaller the slip, the smaller the range of the impact and deflection angle. As shown in Fig. 8, the deflection of  $S_{H_{max}}$  caused by faults F2 and F3 was not as significant as that caused by major faults F1 and F6. In other words, the overall stress distribution and changes in the study area were mainly controlled and influenced by the arc boundary faults.

Deflection in in situ stress orientation is also affected by the rock mechanics properties of the filling material within a fault zone. Hudson and Cooling (1988) propose that if the elastic modulus of the filling materials within a fault is lower than that of the surrounding rocks, the stress orientation will be deflected along the fault's strike; if the elastic modulus is higher, the stress orientation will be deflected perpendicular to the fault's strike; and if the elastic modulus of both are similar, there will be no deflection. All the faults developed in the No. 4 Structure were normal faults. Interpretation of the core observation and well logging data indicated that the filling materials within the fault had a compaction effect but did not strongly crush the rock mass. Since the elastic modulus of the filling materials was lower than that of the surrounding rocks, the influence of filling material in the No. 4 Structure was to deflect  $S_{H_{max}}$  along the fault strike.

## 4.2 In situ stress magnitude

The simulation results of the No. 4 Structure's 3D stress field indicated that for the distribution of  $S_{H_{max}}$  magnitude, the general trend was that it was lower in the west and higher in the east. This was consistent with the trend observed in measured data. The range of the  $S_{H_{max}}$  magnitudes was

mostly 53–88 MPa. Moving from oil series I to oil series V, the magnitude of  $S_{H_{max}}$  increased with depth. The average stress gradient was 1.83 MPa/100 m. At fault peripheries, stresses were lower at about 32–51 MPa (such as F1 and F6 in oil series I in Fig. 9a), and  $S_{H_{max}}$  was reduced by 30% compared to that of the layer. Where fault scale was large (wide slip and long extension, such as F1 and F4), it resulted in a bigger range in low-magnitude zones. At fault intersections, the internal rock mass was more severely crushed and there was a greater reduction in stress magnitude. Faults with different dip had different impacts on the in situ stress distribution, that is, The steeper the dip, the smaller the range in low-magnitude zones caused by the fault; the shallower the dip, the larger the range in low-magnitude zones.

The distribution trend of  $S_{H_{min}}$  magnitude was similar to that of  $S_{H_{max}}$ , that is, lower in the central part and fault zone and higher in the surrounding area. The magnitudes were mainly between 36–65 MPa and the average stress gradient was 1.47 MPa/100 m. For vertical principal stress, the magnitudes were about 70–90 MPa, and the average stress gradient was 2.25 MPa/100 m. Overall, horizontal differential stress did not exceed 30 MPa and was generally below 20 MPa. Again, the distribution trend was one of being lower in the west and higher in the east (Fig. 9b). Within the target layer, if the vertical principal stress is greater than the horizontal stresses, this belongs to the Ia-type of in situ stress (Anderson 1951).

The linear relationships between depth and the No. 4 Structure's  $S_{H_{max}}$  and  $S_{H_{min}}$  and vertical principal stress were ideal (Fig. 10a). Since the vertical principal stress is basically related to burial depth and rock density, their correlation coefficient was highest ( $>0.97$ ). The horizontal stresses were affected by multiple factors including structural form, stratum heterogeneity, and residual tectonic stress. Thus, the heterogeneity was greater than the vertical principal stress and the correlation coefficient was about 0.75. The heterogeneity of the principal stress gradually decreased with increasing depth. For the target layer in the No. 4 Structure, the  $S_{H_{max}}$  and  $S_{H_{min}}$  coefficients were concentrated at 0.83 and 0.64, respectively and that of the lateral pressure coefficient was concentrated at 0.74 (Fig. 10b).

## 4.3 Analysis of inter-strata in situ stress

Inter-strata in situ stress affects the height and direction in which fractures extend and expand, which is important to reservoir modeling. The combined Petrel and ANSYS modeling techniques made it possible for the predicted stress field obtained by numerical simulation to be used as a type of geological information for inputting into the 3D geological model. In turn, the characteristics of the stress field profile could be presented in detail in the Petrel grid (Fig. 11a–d).

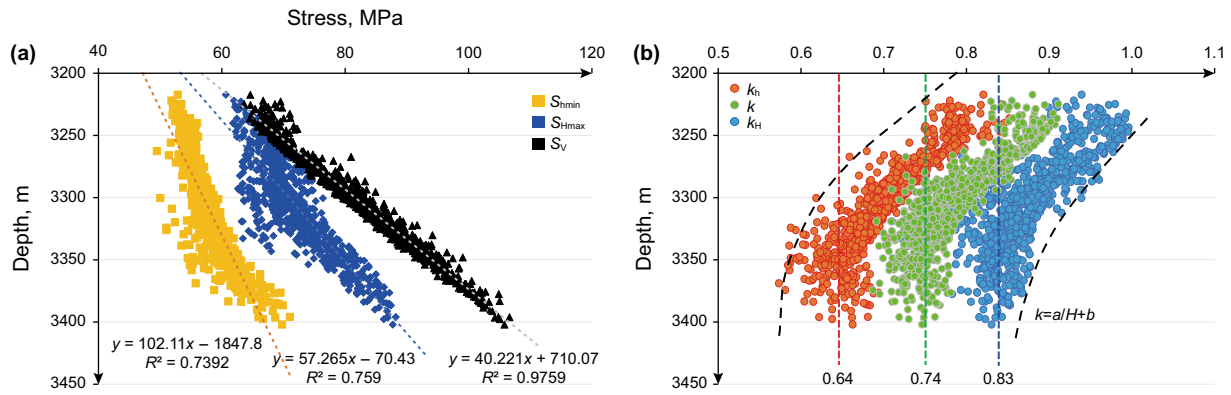


**Fig. 10** **a** Relationship between depth and the No. 4 Structure’s principal stress components. **b** Relationship between depth and the No. 4 Structure’s stress coefficients

In the field profile, the in situ stress magnitudes of the No. 4 Structure varied greatly with significant differences in inter-strata in situ stress. This was because a quantitative relationship exists between the rock mechanics parameters (especially Young’s elastic modulus) and the in situ stress magnitudes. Such inter-strata variations in in situ stress directly relate to the heterogeneity of the reservoir’s rock mechanics parameters (Yan 2007).

Horizontal differential stress is the key factor controlling volumetric fracturing. A complex network of seams is easily formed when the differential stress is small; otherwise, a unidirectional fracture that is parallel to the  $S_{Hmax}$  will form instead. On the other hand, potential extensions of fracture height and length are mainly controlled by the distribution of the minimum principal stress above the fractured sections of the layer (Dong et al. 2005), and the  $S_{Hmax}$  orientation (Zhang et al. 2016), respectively.

The No. 4 Structure was divided into five types of typical stress profile (Types A–E; Fig. 11e), all of which were present in the in situ stress profiles of wells NP43-4942 and NP4-31. As shown in Fig. 11c and d, the stress distribution pattern of Type A was “high–low–high,” meaning that fracturing operations in this area would be limited by the high differential stress (usually greater than 5 MPa) between the upper and lower strata. The possibility of the fracturing seam passing through the layer was small, thereby restricting the scale of the operation. For Type B, the distribution pattern was “low–low–high.” The horizontal differential stress of the upper layer should be less than 4 MPa, while that of the lower layer was larger, meaning that upward fracture extensions would occur easily. Under this scenario, all well sections with lower stress differences would be fractured. Thus, the amount of fluid injected and scale of the operation must be carefully considered.

The distribution pattern of Type C was “high–low–low.” The horizontal differential stresses of the layer above and below were small and large, respectively, such that fracture

extensions tended to be downward. Type D had an inter-strata distribution pattern, with the horizontal differential stress in the range of the well section being small. Nevertheless, variations existed such that it was possible for the fracturing seam to extend either upward and/or downward, while the direction of extension might also change. The distribution pattern of Type E was “low–low–low.” The horizontal differential stress within the well section was small and uniform, which facilitated easy extension of the fracturing seam both upward and downward. At the same time, there was likely to be the formation of a complex network of seams. These were the ideal in situ stress conditions for fracturing operations.

Therefore, the distribution of inter-strata in situ stress must be clearly understood during the period of fracturing operations so that inter-strata fracture extensions could be predicted. Otherwise, sand blockages are likely to occur, resulting in the suspension or even failure of the operation. Also mud losses, and other problems associated with over- and under-pressurized boreholes, might occur. With accurate assessments of the possible extensions of the fractures’ heights and lengths, the scale of operation and deployment of the well network could be determined rationally. When this was done, better results could be obtained from reservoir reconstruction.

## 5 Conclusion

In this study, borehole breakouts and acoustic emission (AE) were used to determine the orientation and magnitude of in situ stress in the No. 4 Structure of Nanpu Sag. Our approach of applying a combined modeling technique using Petrel and ANSYS fully tapped the advantages of both software packages and facilitated the construction of 3D models and heterogeneous rock mechanics fields. These improved the accuracy of simulated results, especially in terms of the

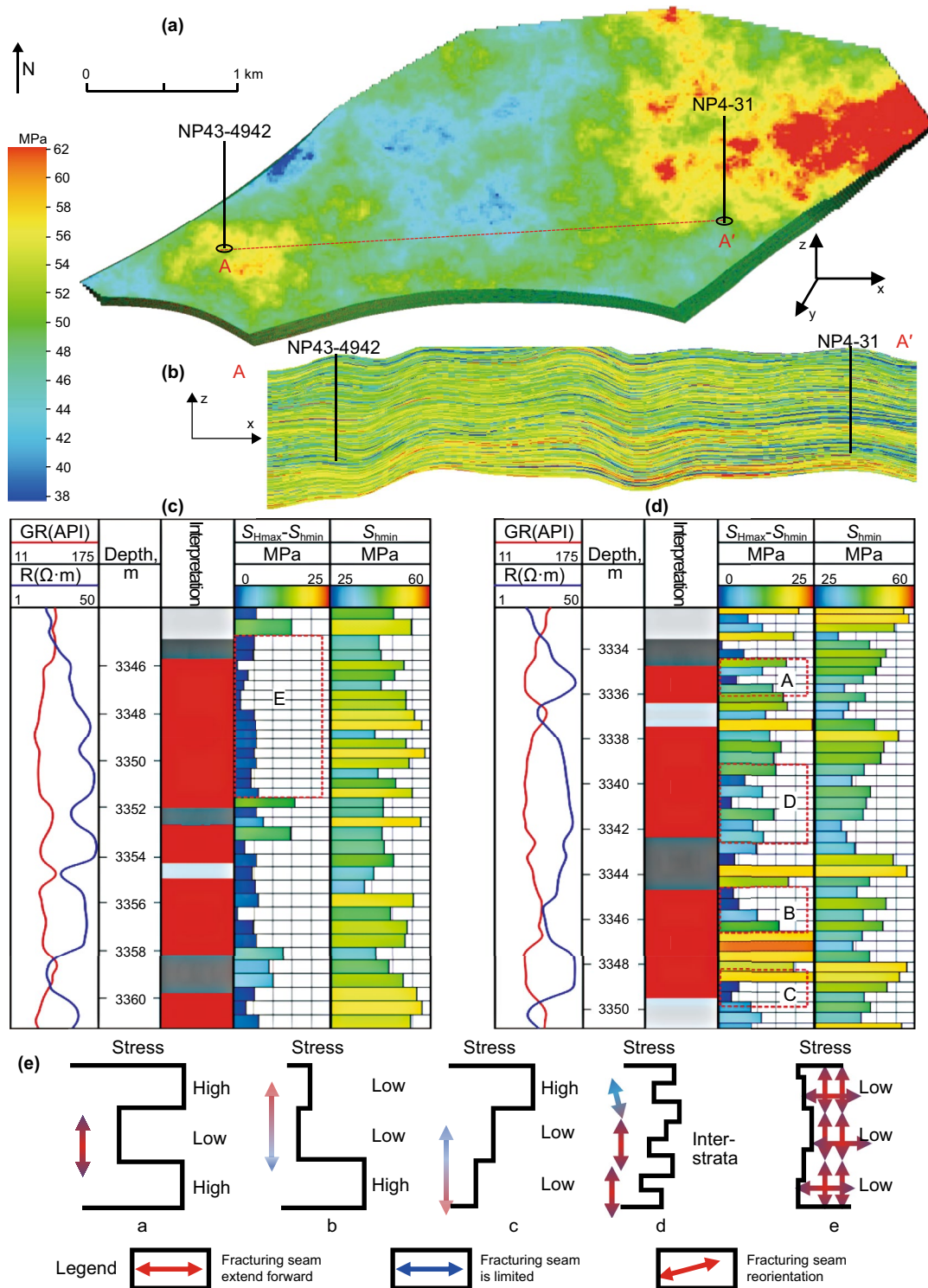


**Fig. 11** No. 4 Structure: in situ stress characteristics and profile types. **a** 3D distribution of  $S_{hmin}$  of the No. 4 Structure. **b** East-west 2D profile of stress difference in the No. 4 Structure. **c** In situ stress profile of well NP43-4942. **d** In situ stress profile of well NP4-31. **e** In situ stress profile types identified from the No. 4 Structure wells

clear presentation of inter-strata in situ stress characteristics. The research results had successfully been applied for oil and gas exploitation by the PetroChina Jidong Oil field

Company. This technique had been demonstrated to be suitable for the comprehensive prediction of the 3D distribution of in situ stress in a heterogeneous reservoir located within

complex fault blocks. However, prediction of the in situ stress could be improved by consideration of fluid and temperature factors, and modeling of the dynamic in situ stress field during development of an oil–gas field.

The following conclusions were made:

1. Prediction of the in situ stress field of the No. 4 Structure could be performed by considering the spatial variation in mechanical parameters, and morphology and occurrence of faults.
2. The simulation results showed that overall orientation of the No. 4 Structure's maximum horizontal stress was NEE–SWW to SEE–NWW, changes of which were mainly controlled and influenced by the arc boundary faults, and that stress magnitude was lower in the north and higher in the south.
3. The in situ stress magnitudes were discrete along surfaces and in profile, and the in situ stress belongs to the Ia-type, that is  $S_v > S_{Hmax} > S_{hmin}$ , and  $S_{hmin} > 0$ .
4. Heterogeneity of the principal stress gradually decreased with increasing depth, and the inter-strata variations in in situ stress were significant and could be divided into five profile types: “high–low–high,” “low–low–high,” “high–low–low,” “inter-strata,” and “low–low–low.”
5. Faults were the most important factors affecting variations in the stress field in reservoirs located within complex fault blocks. They could significantly affect the magnitudes and orientations of the in situ stress field. The boundary faults of the No. 4 Structure significantly influenced the in situ stress of Napu.4 Fault, causing deflections of stress orientation and reductions in stress magnitude. Next the rock mechanics parameters were important, which significantly affected the magnitudes, but not orientations. There was a high linear correlation between the buried depth and the in situ stress magnitudes. Therefore, the critical prerequisites for studying the stress fields of regions with complex fault blocks included the characterization of faults and construction of the heterogeneous rock mechanics field.

**Acknowledgements** This research was financially supported by the National Oil and Gas Major Project (2016ZX05047-003, 2016ZX05014002-006), the National Natural Science Foundation of China (41572124), and the Fundamental Research Funds for the Central Universities (17CX05010).

**Open Access** This article is distributed under the terms of the Creative Commons Attribution 4.0 International License (<http://creativecommons.org/licenses/by/4.0/>), which permits unrestricted use, distribution, and reproduction in any medium, provided you give appropriate credit to the original author(s) and the source, provide a link to the Creative Commons license, and indicate if changes were made.

## References

- Anderson EM. The dynamics of faulting and dyke formation with applications to Britain. 2nd ed. Edinburgh: Oliver; 1951.
- Bell JS. Petro geoscience 2. In situ stresses in sedimentary rocks (part 2): applications of stress measurements. *Geosci Can.* 1996;23(3):135–53.
- Bell JS. In-situ stress and coal bed methane potential in Western Canada. *Bull Can Pet Geol.* 2006;54:197–220.
- Bell JS, Gough DI. Northeast-southwest compressive stress in Alberta: evidence from oil wells. *Earth Planet Sci Lett.* 1979;45:475–82. [https://doi.org/10.1016/0012-821x\(79\)90146-8](https://doi.org/10.1016/0012-821x(79)90146-8).
- Binh NTT, Tokunaga T, Son HP, et al. Present-day stress and pore pressure fields in the Cuu Long and Nam Con Son basins, offshore Vietnam. *Mar Pet Geol.* 2007;24:607–15. <https://doi.org/10.1016/j.marpetgeo.2007.04.002>.
- Brooke-Barnett S, Flottmann T, Paul PK, et al. Influence of basement structures on in situ stresses over the Surat Basin, southeast Queensland. *J Geophys Res Solid Earth* 2015. <https://doi.org/10.1002/2015JB011964>.
- Brown ET, Hoek E. Trends in relationships between measured in situ stresses and depth. *Int J Rock Mech Min Sci.* 1978;15:211–5. [https://doi.org/10.1016/0148-9062\(78\)91227-5](https://doi.org/10.1016/0148-9062(78)91227-5).
- Cao CJ (2005). Tectonic stress field analysis and application in the northwest Sichuan Basin. PhD dissertation, Graduate School of Chinese Academy of Geological Sciences, Beijing. 2005. (in Chinese).
- Chen H, Wang XM, Zhao LX, et al. Study of inversion for third order elastic constants and in situ stress by multifrequency dispersion of cross dipole sonic logging. *Chin J Geophys.* 2009a;52:1663–74. <https://doi.org/10.1002/cjg2.1395> (in Chinese).
- Chen JD, Ma SP, Liu SJ, et al. An experimental study of the failure process of en-echelon fault structure using the digital speckle correlation. *Chin J Geophys* 2005;48(6):1350–6. <https://doi.org/10.1002/cjg2.790> (in Chinese).
- Chen M, Yan Z, Yan J, et al. Experimental study of influence of loading rate on kaiser effect of different lithological rocks. *Chin J Rock Mech Eng.* 2009b;28:2599–604. <https://doi.org/10.13225/j.cnki.jccs.2017.1003> (in Chinese).
- Chiang FP, Mao LT. Development of interior strain measurement techniques using random speckle patterns. *Meccanica.* 2015;50(2):401–10. <https://doi.org/10.1007/s11012-014-0048-1> (in Chinese).
- Dai JS. Structural analysis of oil province. Dongying: Petroleum University Press; 2002. p. 167–88 (in Chinese).
- Dai JS, Wang XT, Zong-Zhen JI, et al. Structural stress field of funing sedimentary period and its control on faults in the east of south fault terrace in Gaoyou Sag. *J China Univ Pet.* 2011;35(2):1–5. <https://doi.org/10.3969/j.issn.1673-5005.2011.02.001> (in Chinese).
- Dai JS, Zou J, Zhao XZ, et al. Fault characteristics interpretation of Ek–E<sub>s4</sub> sedimentary period in Hexiwiu tectonic belt through stress field simulation. *Nat Gas Geosci.* 2014;25(10):1529–36. <https://doi.org/10.11764/j.issn.1672-1926.2014.10.1529> (in Chinese).
- Dai JS, Liu JS, Yang HM, et al. Numerical simulation of stress field of Fu-2 member in Tongcheng fault zone and development suggestions. *J China Univ Pet: Ed Nat Sci.* 2016;40:1–9. <https://doi.org/10.3969/j.issn.1673-5005.2016.01.001> (in Chinese).
- Dai LM, Li SZ, Lou DS, et al. Numerical modeling on the stress field in the Huanghua depression, Bohai Bay basin. *Chin J Geophys.* 2013;56(3):929–42. <https://doi.org/10.6038/cjg20130321> (in Chinese).

- Ding YC, Zhang DL (1991). An acoustic emission Kaiser effect discrimination method for in-situ stress measurement. *Geostress Field Test Appl Papers*. 1991;10(4):313–26 (in Chinese).
- Dong JH, Liu P, Wang W. Application of in situ stress profile to hydraulic fracturing. *J Northeast Pet Univ*. 2005;29:40–2. <https://doi.org/10.1016/j.molcatb.2005.02.001> (in Chinese).
- Dong YX, Xiao L, Zhou HM, et al. The Tertiary evolution of the prolific Nanpu Sag of Bohai Bay Basin, China: constraints from volcanic records and tectono-stratigraphic sequences. *GSA Bull*. 2010;122:609–26. <https://doi.org/10.1130/b30041.1> (in Chinese).
- Ding WL, Fan TL, Huang XB, et al. Upper Ordovician paleo tectonic stress field simulating and fracture distribution forecasting in Tazhong area of Tarim Basin, Xinjiang, China. *Geol Bull China*. 2011;30(4):588–94 (in Chinese).
- Ding W, Zeng W, Wang R, et al. Method and application of tectonic stress field simulation and fracture distribution prediction in shale reservoir. *Earth Sci Front*. 2016;23(2):63–74 (in Chinese).
- Engelder T. *Stress regimes in the lithosphere*. Princeton: Princeton University Press; 1993. p. 23–30. <https://doi.org/10.1515/9781400863150>.
- Eshiet KI, Sheng Y. The performance of stochastic designs in wellbore drilling operations. *Pet Sci*. 2018;15(2):335. <https://doi.org/10.1007/s12182-018-0219-0>.
- Fan YR, Wei ZT, Chen XL, et al. Study on formation stress calculation and its influential factors based on logging data. *Well Log Technol* 2009;33:415–20. [https://doi.org/10.1016/s1003-6326\(09\)60084-4](https://doi.org/10.1016/s1003-6326(09)60084-4) (in Chinese).
- Farrell NJC, Healy D, Taylor CW. Anisotropy of permeability in faulted porous sandstones. *J Struct Geol*. 2014;63:50–67. <https://doi.org/10.1016/j.jsg.2014.02.008>.
- Finkbeiner T, Zoback M, Flemings P, et al. Stress, pore pressure, and dynamically constrained hydrocarbon columns in the South Eugene Island 330 field, northern Gulf of Mexico. *AAPG Bull*. 2001;85:1007–31.
- Gong ZS. *Giant offshore oil and gas fields in China*. Beijing: Petroleum Industry Press; 1997 (in Chinese).
- Guo R, Yao L, Ren D. Simulation of three-dimensional tectonic stress fields and quantitative prediction of tectonic fracture within the Damintun Depression, Liaohe Basin, northeast China. *J Struct Geol*. 2016;86:211–23. <https://doi.org/10.1016/j.jsg.2016.03.007>.
- Haghi AH, Kharrat R, Asef MR, et al. Present-day stress of the central Persian Gulf: implications for drilling and well performance. *Tectonophysics*. 2013;608:1429–41. <https://doi.org/10.1016/j.tecto.2013.06.001>.
- He SM, Wang W, Shen H, et al. Factors influencing wellbore stability during underbalanced drilling of horizontal wells when fluid seepage is considered. *J Nat Gas Sci Eng* 2015;23:80–9 (in Chinese).
- Hoda D, Morteza NT, Amin S, et al. Geo-mechanical modeling and selection of suitable layer for hydraulic fracturing operation in an oil reservoir (south west of Iran). *J Afr Earth Sci* 2015;111:409–20. <https://doi.org/10.1016/j.jafrearsci.2015.08.001>.
- Holcomb DJ. Observations of the Kaiser Effect under multiaxial stress states: implications for its use in determining in situ stress. *Geophys Res Lett*. 1993;20:2119–22. <https://doi.org/10.1029/93gl01270>.
- Hudson JA, Cooling CM. In Situ, rock stresses and their measurement in the U.K.—Part I. The current state of knowledge. *Int J Rock Mech Min Sci Geomech Abstr*. 1988;25:363–70. [https://doi.org/10.1016/0148-9062\(88\)90976-x](https://doi.org/10.1016/0148-9062(88)90976-x).
- Jiu K, Ding WL, Huang WH, et al. Simulation of paleotectonic stress field within Paleogene shale reservoirs and prediction of favorable zones for fracture development within the Zhanhua Depression, Bohai Bay Basin, east China. *J Pet Sci Eng*. 2013;110:119–31 (in Chinese).
- Ju W, Sun WF. Tectonic fractures in the lower cretaceous Xiagou formation of Qingxi oilfield, Jiuxi basin, NW China. Part two: numerical simulation of tectonic stress field and prediction of tectonic fractures. *J Pet Sci Eng*. 2016;146:626–36. <https://doi.org/10.1016/j.petrol.2016.05.002>.
- Ju W, Sun WF, Ma XJ, et al. Tectonic stress accumulation in Bohai-Zhangjiakou seismotectonic zone based on 3d visco-elastic modelling. *J Earth Syst Sci*. 2016;125(5):1021–31. <https://doi.org/10.1007/s12040-016-0706-x> (in Chinese).
- Ju W, Shen J, Qin Y, et al. In-situ stress state in the linxing region, eastern ordos basin, china: implications for unconventional gas exploration and production. *Mar Pet Geol*. 2017;86:67–78 (in Chinese).
- Kang H, Zhang X, Si L, et al. In-situ stress measurements and stress distribution characteristics in underground coal mines in China. *Eng Geol*. 2010;116:333–45. <https://doi.org/10.1016/j.enggeo.2010.09.015> (in Chinese).
- Kingdon A, Fellgett MW, Williams JDO. Use of borehole imaging to improve understanding of the in situ stress orientation of Central and Northern England and its implications for unconventional hydrocarbon resources. *Mar Pet Geol*. 2016;73:1–20. <https://doi.org/10.1016/j.marpetgeo.2016.02.012>.
- Lehtonen A, Cosgrove JW, Hudson JA, et al. An examination of in situ, rock stress estimation using the Kaiser effect. *Eng Geol*. 2012;124:24–37.
- Lei G, Dai J, Yujie MA, et al. Numerical simulation of the current stress field and reservoir fracture in keshen 3d area of kuqa depression. *Pet Geol Oilfield Dev Daqing*. 2015;34(1):18–23. <https://doi.org/10.1631/jzus.a1000209> (in Chinese).
- Li LI, Zou Z, Zhang Q. Current situation of the study on kaiser effect of rock acoustic emission in in situ stress measurement. *Coal Geol Explor*. 2011a;39(1):341–92 (in Chinese).
- Li SB, Dou TW, Dong DR, et al. Stress state of bottom-hole rocks in underbalanced drilling. *Acta Pet Sin*. 2011b;32:329–34 (in Chinese).
- Li Y, Tang DZ, Xu H, et al. In-situ stress distribution and its implication on coalbed methane development in Liulin area, eastern Ordos Basin, China. *J Pet Sci Eng*. 2014;122:488–96. <https://doi.org/10.1016/j.petrol.2014.08.010> (in Chinese).
- Liu C, Huang XB, Fan TL, et al. The simulation of present tectonic stress field and the prediction of tectonic fractures of Ordovician in Tazhong Area, Tarim Basin. *Xinjiang Pet Geol*. 2008;29:475–7 (in Chinese with English abstract).
- Liu QJ, Yan XZ, Yang XJ. Application of optimization back-analysis method in reservoir stress and fracture study. *Pet Drill Tech*. 2009;37:26–31. [https://doi.org/10.1016/0378-1119\(92\)90673-d](https://doi.org/10.1016/0378-1119(92)90673-d) (in Chinese).
- Liu R, Liu JZ, Zhu WL, et al. In situ stress analysis in the Yinggehai Basin, northwestern South China Sea: implication for the pore pressure–stress coupling process. *Mar Pet Geol*. 2016;77:341–52. <https://doi.org/10.1016/j.marpetgeo.2016.06.008> (in Chinese).
- Liu X, Fu RS, Yang GH, et al. Deformation field an tectonic stress filed constrained by GPS observations in North China. *J Geodest Geodyn ICS*. 2006;26(3):33–8. <https://doi.org/10.1007/s11442-006-0415-5> (in Chinese).
- Lu SK, Wang D, Li YK, et al. Research on three-dimensional mechanical parameters' distribution of the tight sandstone reservoirs in Daniudi Gasfield. *Nat Gas Geosci*. 2015;26:1844–50. <https://doi.org/10.11764/j.issn.1672-1926.2015.10.1844> (in Chinese).
- Lu Y, Lu RS. Full field deformation fast measurement based on digital image speckle correlation. *J Electron Meas Instrum*. 2016;30(2):1828–37 (in Chinese).
- Lommatzsch M, Exner U, Gier S, et al. Dilatant shear bandformation and diagenesis in calcareous, arkosic sandstones, Vienna Basin (Austria). *Mar Pet Geol*. 2015;62:144–60. <https://doi.org/10.1016/j.marpetgeo.2015.02.002>.



- Mann P, Hempton MR, Bradley DC, et al. Development of pull-apart basins. *J Geol.* 1983;91(5):529–54. <https://doi.org/10.1086/628803>.
- Mao DF, Zhang MH, Yu Y, et al. Analysis of spudcan–footprint interaction in a single soil with nonlinear FEM. *Pet Sci* 2015a;12(1):148–56. <https://doi.org/10.1007/s12182-014-0007-4>.
- Mao LT, Zuo JP, Yuan ZX, et al. Full-field mapping of internal strain distribution in red sandstone specimen under compression using digital volumetric speckle photography and X-ray computed tomography. *J Rock Mech Geotech Eng.* 2015b;7:136–46. <https://doi.org/10.1016/j.jrmge.2015.01.003> (in Chinese).
- Mizuta Y, Sano O, Ogino S, et al. Three dimensional stress determination by hydraulic fracturing for underground excavation design. *Int J Rock Mech Min Sci Geomech Abstr.* 1987;24(1):15–29. [https://doi.org/10.1016/0148-9062\(87\)91228-9](https://doi.org/10.1016/0148-9062(87)91228-9).
- Nelson PH. Pore- throat sizes in sandstones, tight sandstones, and shales. *AAPG Bull.* 2009;93(3):329–40.
- Plumb RA, Hickman SH. Stress-induced borehole elongation: a comparison between the four-arm dipmeter and the borehole televiewer in the Auburn Geothermal Well. *J Geophys Res.* 1985;90:5513–21. <https://doi.org/10.1029/jb090ib07p05513>.
- Rajabi M, Sherkati S, Bohloli B, et al. Subsurface fracture analysis and determination of in situ stress direction using FMI logs: an example from the Santonian carbonates (Ilam Formation) in the Abadan Plain, Iran. *Tectonophysics.* 2010;492:192–200. <https://doi.org/10.1016/j.tecto.2010.06.014>.
- Savage WZ, Swolfs HS, Amadei B. On the state of stress in the near-surface of the earth's crust. *Pure appl Geophys.* 1992;138:207–28. <https://doi.org/10.1007/BF00878896>.
- Sibson R (1994) Crustal stress, faulting and fluid flow. In: Parnell, J. (Ed.), *Geofluids: origin, migration and evolution of fluids in sedimentary basins*, vol. 78. Geological Society of London, Special Publication. pp 69–84.
- Shui TH, Loon AJ, Lin V, et al. Seismites in the Dasheng group: new evidence of strong tectonic and earthquake activities of the Tanlu fault zone. *Sci China.* 2016;59(3):601–18. <https://doi.org/10.1007/s11430-015-5221-4> (in Chinese).
- Tian YP, Liu X, Li X, et al. Finite element method of 3-D numerical simulation on tectonic stress field. *Earth Sci J China Univ Geoscience.* 2011;36:375–80. <https://doi.org/10.3799/dqkx.2011.041> (in Chinese).
- Tingay M, Hills RR, Morley CK, et al. Present-day stress and neotectonics of Brunei: implications for petroleum exploration and production. *AAPG Bull.* 2009;93(1):75–100.
- Tingay MRP, Morley CK, Hillis RR, et al. Present-day stress orientation in Thailand's basins. *J Struct Geol.* 2010;32:235–48. <https://doi.org/10.1016/j.jsg.2009.11.008>.
- Wang BF, Dai JS, Cheng RH, et al. Present ground stress in Dina gas field. *Xinjiang Pet Geol.* 2007;28(4):470–1. [https://doi.org/10.1016/S1872-5813\(07\)60034-6](https://doi.org/10.1016/S1872-5813(07)60034-6) (in Chinese).
- Wang K (2014). Quantitative description of fracture of clastic reservoir in gram gas field. PhD dissertation, China University of Petroleum, Tsingtao 2014 (in Chinese).
- Wang K, Dai JS, Feng JW, et al. Research on reservoir rock mechanical parameters of Keshen foreland thrust belt in Tarim Basin. *J China Univ Pet Ed Nat Sci.* 2014. <https://doi.org/10.3969/j.issn.1673-5005.2014.05.004>.
- Wang RF, Chi YG, Zhang L, et al. Comparative studies of microscopic pore throat characteristics of unconventional super-low permeability sandstone reservoirs: examples of Chang 6 and Chang 8 reservoirs of Yanchang Formation in Ordos Basin, China. *J Pet Sci Eng.* 2018;160:72–90. <https://doi.org/10.1016/j.petrol.2017.10.030>.
- Wang S, Dai J, Fu X, et al. Numerical simulation research on current stress of Es3 of the 5th block of Bonan oilfield and analysis of its influence factors. *Pet Geol Recov Effic.* 2016;23(3):26–32 (in Chinese).
- Wang XJ, Peng SM, Lv BX, et al. Researching earth stress field using cross dipole acoustic logging technology. *J China Univ Pet Nat Sci Ed.* 2008;32:42–6 (in Chinese).
- Xie RC, Zhou W, Tao Y, et al. Application of finite element analysis in the simulation of the in situ stress field. *Pet Drill Technol.* 2008;36:60–3 (in Chinese).
- Yan P (2007). The earth stress calculation using well logging data and its applied research in piedmont structure. M.E. thesis, University of Petroleum, Beijing. 2007 (in Chinese).
- Yang XQ, Shi XB, Xu HH. Numerical modeling of the current tectonic stress field. *Chin J Geophys Taiwan Strait Adjac Reg.* 2012;55:2307–18 (in Chinese).
- Yang YY, Zhao P, Zheng HG, et al. Evidence of holocene activity discovered in Anhui Ziyangshan segment of Tanlu fault zone. *Seismol Geol.* 2017;39(4):644–55. <https://doi.org/10.3969/j.issn.0253-4967.2017.04.002> (in Chinese).
- Yu X, Hou G, Li Y, et al. Quantitative prediction of tectonic fractures of lower Jurassic Ahe Formation sandstones in Dibeigasfield. *Earth Sci Front.* 2016;23:240–52. <https://doi.org/10.13745/j.esf.2016.01.022> (in Chinese).
- Zang A, Stephansson O. *Stress field of the Earth's Crust.* Berlin: Springer; 2009. p. 131–92.
- Zeng LB, Su H, Tang XM, et al. Fractured tight sandstone oil and gas reservoirs: a new play type in the Dongou depression, Bohai Bay Basin, China. *AAPG Bull.* 2013;97(3):363–77 (in Chinese).
- Zeng Q, Liu T, Shen Y, et al. The tanlu fault zone and gold ore metallogenesis in eastern china. *Int Geol Rev.* 2001;43(2):176–90. <https://doi.org/10.1080/00206810109465006> (in Chinese).
- Zhang CM (2010). Tectono-sedimentary analysis of Nanpu sag in the Bohaiwan Basin. PhD dissertation, China University of Geosciences, Beijing. 2010 (in Chinese).
- Zhang ZQ, Zhang YM, Bu XQ, et al. A Study of in situ stress direction change during waterflooding in the low permeability reservoirs. *J Peking Univ (Ed Nat Sci).* 2016;52:861–70. <https://doi.org/10.13209/j.0479-8023.2015.140> (in Chinese).
- Zhang ZY, Wu ML, Chen QC, et al. Review of in situ stress measurement methods. *J Henan Polytech Univ (Ed Nat Sci).* 2012;31:305–10 (in Chinese).
- Zhao K, Yan DQ, Zhong CH, et al. Comprehensive analysis method and experimental verification for in situ stress measurement by acoustic emission tests. *Chin J Geotech Eng.* 2012;34(8):1403–11 (in Chinese).
- Zhu CH, Wang WF, Wang QZ, et al. Numerical simulation of structural strain for Turbidite Sands Reservoirs of low permeability. *J Jilin Univ (Earth Sci Ed).* 2016;46:1580–8. <https://doi.org/10.13278/j.cnki.jjuese.201605306> (in Chinese).
- Zoback MD, Barton CA, Brudy M, et al. Determination of stress orientation and magnitude in deep wells. *Int J Rock Mech Min Sci.* 2003;40:1049–76. <https://doi.org/10.1016/j.ijrmms.2003.07.001>.
- Zoback MD. *Reservoir geomechanics.* Cambridge: Cambridge University Press; 2007.